PHYSICAL REVIEW B **93**, 060409(R) (2016)

Emergence of skyrmions from rich parent phases in the molybdenum nitrides

Wei Li,[1] Chiming Jin,[2,3] Renchao Che,[4] Wensen Wei,[2,3,5] Langsheng Lin,[2,3] Lei Zhang,[2,3] Haifeng Du,[2,3,5] Mingliang Tian,[2,3,5] and Jiadong Zang[6,*]

[1]*State Key Laboratory of Functional Materials for Informatics and Shanghai Center for Superconductivity, Shanghai Institute of Microsystem and Information Technology, and CAS-Shanghai Science Research Center, Chinese Academy of Sciences, Shanghai 200050, China*

[2]*High Magnetic Field Laboratory, Chinese Academy of Science (CAS), Hefei 230031, China*

[3]*Collaborative Innovation Center of Advanced Microstructures, Nanjing University, Jiangsu 210093, China*

[4]*Laboratory of Advanced Materials, Department of Materials Science, Collaborative Innovation Center of Chemistry for Energy Materials, Fudan University, Shanghai 200438, China*

[5]*Hefei National Laboratory for Physical Science at Microscale and Department of Physics, University of Science and Technology of China, Hefei 230026, China*

[6]*Department of Physics and Materials Science Program, University of New Hampshire, Durham, New Hampshire 03824, USA*

(Received 25 March 2015; revised manuscript received 9 February 2016; published 26 February 2016)

We report a new family of skyrmion materials originated from the antisymmetric Dzyaloshinskii-Moriya (DM) interactions. Based on the symmetric tensor technique, the molybdenum nitrides with the β-manganese structure, A_2Mo_3N with A = Fe, Co, Rh, are predicted to support the skyrmion phase. This predication is directly proved in doped $Fe_xCo_{1-x}Rh_{0.5}Mo_3N$ components by high-resolution Lorentz transmission electron imaging. Interestingly, the parent compounds Fe_2Mo_3N, Co_2Mo_3N, and Rh_2Mo_3N exhibit ferromagnetic, antiferromagnetic, and possible superconducting orderings, respectively. Magnetism in these parent phases is theoretically clarified by the first-principle calculations, where the corrected nature of the magnetism is revealed.

DOI: 10.1103/PhysRevB.93.060409

The magnetic skyrmion is a swirlinglike spin texture with nontrivial topology triggering enormous activity with the target of developing new memory and logic devices [1]. It was first discovered in metallic alloy MnSi by neutron scattering [2], and later confirmed in heavy semiconductor $Fe_{0.5}Co_{0.5}Si$ by Lorentz transmission electron microscopy (TEM) [3]. Both materials belong to the same lattice class of B20, a noncentrosymmetric binary structure in the Strukturbericht symbol scheme. Subsequent investigation proved the emergence of skyrmions is a common feature in other B20 magnets such as FeGe and Cu_2OSeO_3 [4–6]. The continuing discovery of more skyrmion materials is unambiguously an important and urgent job for the development of the skyrmion physics.

Skyrmions in magnetic materials can be stabilized by various interactions, such as the Dzyaloshinskii-Moriya (DM) interaction [4], frustrated exchange interaction [7], and four-spin exchange interactions [8]. The DM interaction is the physics behind noncentrosymmetric B20 compounds, and it has evident advantages over other interactions because skyrmions, originated from this coupling, have small and tunable size [9], fixed unique chirality [1], and extra stability even in highly confined geometries [10]. In B20 compounds, the complex distributions of atoms in each unit cell dramatically bring down the symmetry though this class belongs to the cubic crystal system. Thus the point group of B20 compounds is the tetartoidal T group, the one with lowest symmetry in the cubic system. The inversion symmetry is missing, resulting in the presence of DM interaction [11,12], which favors a perpendicular alignment of spins. The competition between DM coupling and the Heisenberg exchange induces the spin helices under low magnetic field and skyrmions at certain temperature-field window [4]. Notably, early theoretical investigations have proved that DM interaction may exist in a much wider range of materials without inversion symmetry [13,14]. More skyrmion materials are expected. Here, we report on a family of skyrmion materials, the molybdenum nitrides. The family shows the same Hamilton to the conventional B20 compounds, and more complex orderings including ferromagnetism, antiferromagnetism, superconductivity, and skyrmions.

To guide the search of skyrmion materials, it is instructive to classify all possible skyrmion lattices by symmetry. Being similar to the phenomenological theory introduced by Bogdanov *et al.* [15], the technique of symmetric tensor is employed [16,17], and the classification of point groups hosting skyrmions is achieved (see Supplemental Material [18]). Based on the symmetry analysis, we focus on the O group, which manifests the same spin interactions as the familiar B20 compounds. We successfully find a promising family, A_2Mo_3N with A = Fe, Co, Rh, and their alloys, in this group.

The pure A_2Mo_3N with A = Fe, Co, Rh, shown in Fig. 1(a), has the filled β-manganese structure with the space group $P4_132$ [19–21], where atoms A lie on the 8c positions of a cubic unit cell forming a single (10, 3)-a network [22]. The space within this network is filled by corner-shared Mo_6N octahedra.

These molybdenum nitrides have been reported to be ferromagnetic [19–21]. But both molybdenum and magnetic atoms, Fe, Co, and Rh, are heavy so that large spin-orbital coupling is expected in this family, indicating the potential to host significant DM coupling, and skyrmions in consequence. By carefully checking magnetization data in the literature [21], we found the composition $Fe_xCo_{1.5-x}Rh_{0.5}Mo_3N$ vaguely shows similar behavior as the B20 compounds, which becomes our focus. Three polycrystalline $Fe_xCo_{1.5-x}Rh_{0.5}Mo_3N$ alloys with x = 1.0, 0.5, and 0.3 are synthesized by the reductive

*Jiadong.Zang@unh.edu

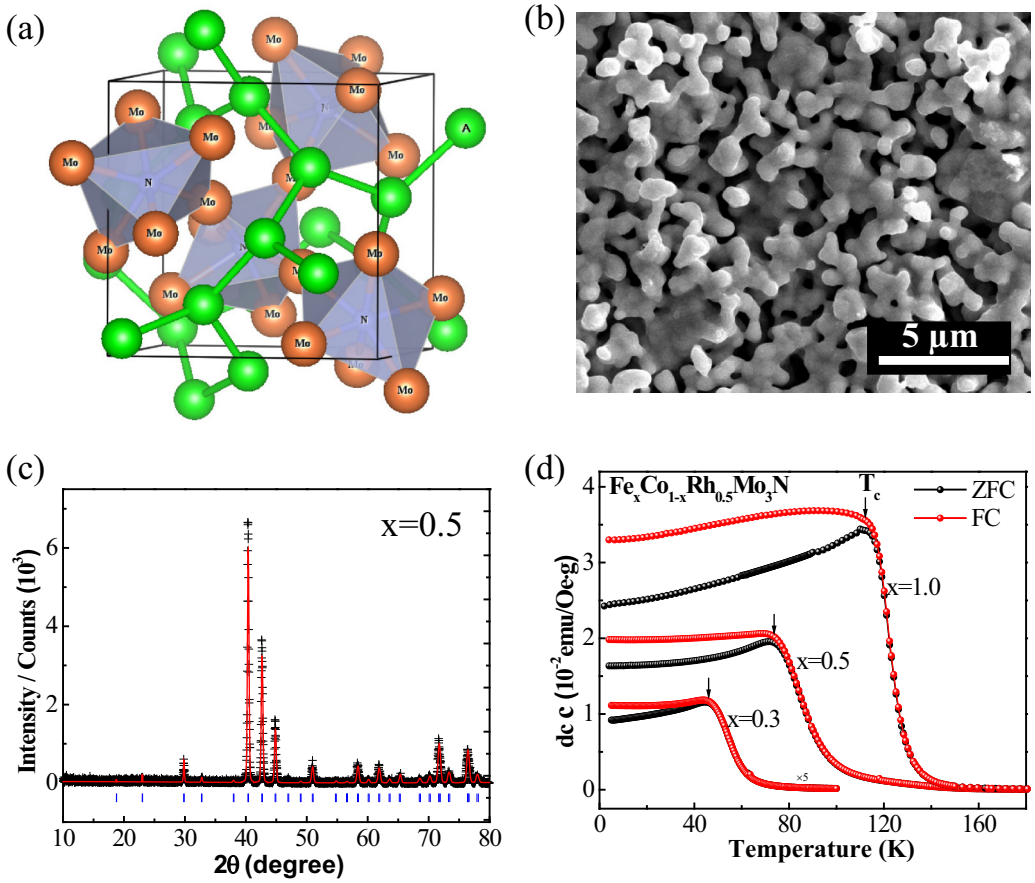

FIG. 1. (a) Schematic crystal structure of the filled β-manganese structural A_2Mo_3N (A = Co, Fe, and Rh). (b) Scanning electron microscopy (SEM) image of the sample. (c) Observed (+) and calculated (red lines) x-ray powder diffraction profiles for the sample. Tick marks indicate positions of allowed reflections for the diffraction. No impurity is observed. (d) Temperature dependence of the dc susceptibility.

nitridation of a binary oxides mixture [19–21]. Figure 1(b) displays a typical scanning electron microscopy (Helios, NanoLab 600i, FEI company) image of $x = 0.5$ component. The sample is composed of inhomogeneous submicrometer grains with irregular shapes and broad size distribution. Such morphology has an important effect on the magnetic properties. Figure 1(c) shows the x-ray data for the $x = 0.5$ component, from which a pure phase is identified. Similar x-ray data are both observed in the other two components, indicating the expected structure without any mixed phase.

The temperature dependence of the dc susceptibility, $\chi = m/H$ with the magnetization m and the external magnetic field $H = 100$ Oe, is shown in Fig. 1(d). The magnetization measurements were carried out by a Quantum Design PPMS device. Under zero field cooling (ZFC), all $\chi(T)$ curves show a peak around the critical temperature T_c. This peak was extensively observed in B20 helimagnets such as MnSi [23], FeGe [24], and $Fe_xCo_{1-x}Si$ [25], where the emergent chiral fluctuating state close to T_c plays an important role [26]. Under field cooling (FC), the peak is smeared out by H [27]. The difference between the ZFC and FC measurements is likely glassy behavior due to frustration between grains with opposite chirality, as demonstrated in MnSi thin films [28].

Although peaks in $\chi(T)$ curves suggest the possible helimagnetic nature of molybdenum nitrides, there are countless other nonhelical magnetic systems with glassy behavior showing similar peaks [29]. To conclusively prove the presence of skyrmions in these materials, real space magnetic imaging by high-resolution Lorentz TEM of JEOL-2100F with a liquid-nitrogen cooling holder (Gatan, Cryo-Transfer Holder) is performed. Here, we only chose the $x = 1.0$ component since its critical temperature is higher than the temperature limit of our TEM equipment. Several polycrystalline samples are fabricated and a typical Lorentz TEM image is shown in Fig. 2 (more images can be found in Fig. S1 [18]). The thin plate with thickness 110 nm is composed of three irregular grains [Fig. 2(a)]. Dot defects and weak strain contrast are simultaneously observed in the sample. Magnetic field H is applied perpendicular to the plate plane. Figures 2(b)–2(e) show typical spin textures under increasing H measured at the lowest temperature possible, $T = 105$ K, of our Lorentz TEM, where the in-plane magnetic moments are obtained by the magnetic transport-of-intensity equation (TIE) analysis (see details in Fig. S2 [18]). At zero field, spin helices are clearly observed, marked as region A in Fig. 2(b). The modulation period is about 110 nm. In contrast to the homogeneous helical domains in single-crystal B20 compounds [3], these spin helices only have limited length compliant with the grain boundaries, indicating the important role of finite size effect and sample quality. Additionally, some skyrmionlike magnetic structures with weaker contrast are simultaneously observed, marked as region B in Fig. 2(b). The presence of these messy

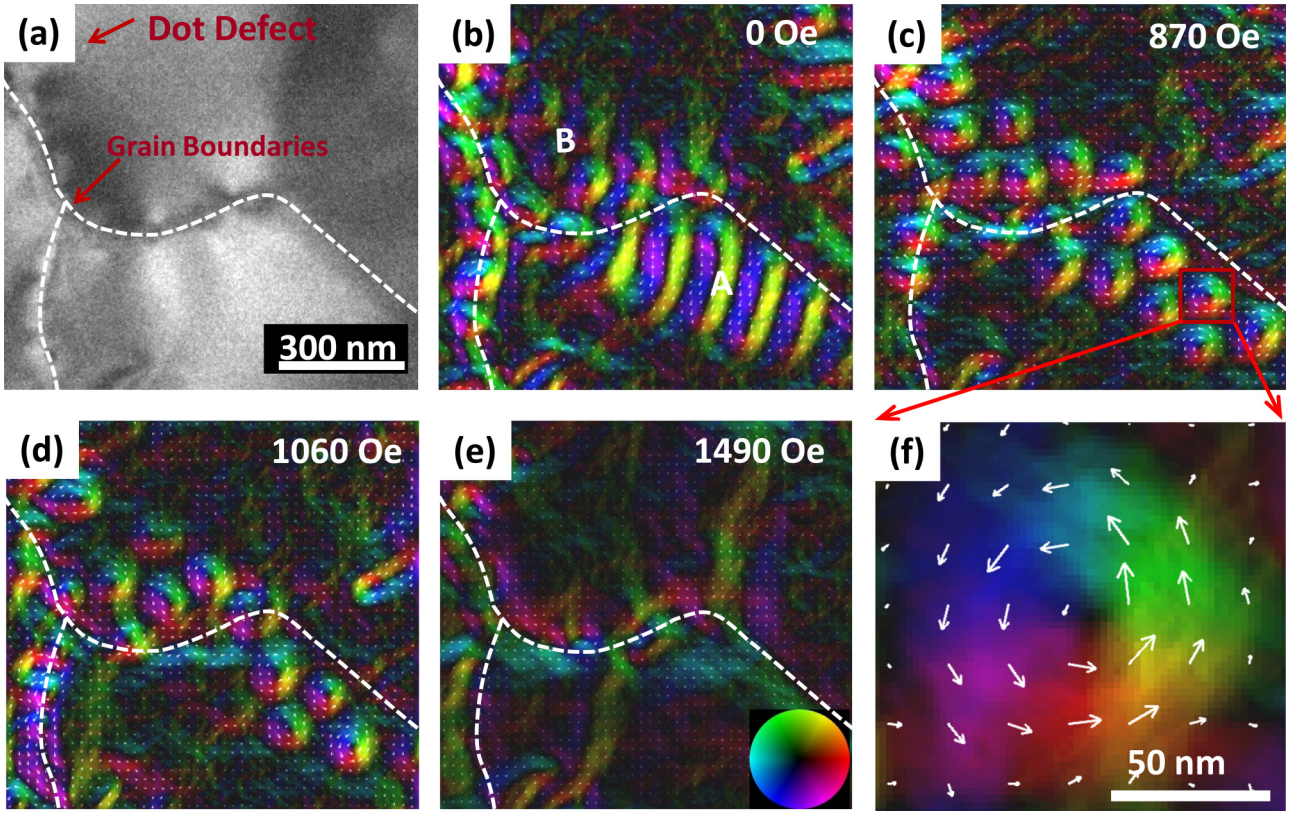

FIG. 2. Variations of spin texture with magnetic field in the $x = 1.0$ sample at $T = 105$ K. (a) TEM image of the sample; the grain boundaries are marked as dotted white lines. (b–h) Field dependence of the spin textures. The color wheel in (e) represents the magnetization direction. Small white arrows represent the in-plane magnetization direction at each point.

spin textures is consistent with the broadened phase boundaries inferred by the ac susceptibility measurements.

At $H \sim 870$ Oe, both helices and the skyrmionlike domains evolve to perfect Bloch skyrmions [Figs. 2(c) and 2(f)]. Skyrmions with nearly identical size to the helix period are closely packed and form a cluster state. Higher fields above $H \sim 1060$ Oe melt the cluster state into isolated skyrmions confined in the same regions [Fig. 2(d)], and finally polarize all the magnetic moments when $H \sim 1490$ Oe [Fig. 2(e)]. This experimental observations show a good agreement with that in the thin plate including $Fe_{0.5}Co_{0.5}Si$ and FeGe [3,5].

Asides from the Lorentz TEM images, the ac susceptibility (χ_{ac}) measurement was further performed to identify the skyrmion phase and build the common phase diagram in the T-H space. Clear skyrmion signals in the ac $\chi(H)$ data are found in the components $x = 0.3$ and 0.5 (see the details in Figs. S3–S5 [18]). Interestingly, it lacks direct skyrmion signals for the $x = 1.0$ bulk sample. But skyrmions are still observed by the Lorentz TEM in the two-dimensional films, reinforcing the positive role of dimension reduction in stabilizing the skyrmion phase [5]. Conclusively, the Lorentz TEM observation together with the magnetization and susceptibility measurements unambiguously prove the helimagentic nature of these molybdenum nitrides.

Not only the alloys $Fe_xCo_{1-x}Rh_{0.5}Mo_3N$ exhibit nontrivial topologies, but also their parent compounds, A_2Mo_3N with $A =$ Fe, Co, Rh, present rich orderings. Although attempts of growing Fe_2Mo_3N end up as a failure, we have successfully synthesized two pure components, Co_2Mo_3N and Rh_2Mo_3N, by using the reductive nitridation of a binary oxides mixture [19–21]. Figure 3(a) shows the $m(T)$ curves of Co_2Mo_3N at a magnetic field $H = 1$ kOe, where they show the typical antiferromagnetism with the Néel temperature $T_N = 115$ K. But, below the critical temperature $T_A = 42$ K, the magnetization of Co_2Mo_3N increases with the increased temperature, which might be relevant to the paramagnetic phase of small grains. Figure 3(b) shows the temperature dependence of Rh_2Mo_3N's magnetization. The magnetization was measured with zero field cooling process (ZFC) and field cooling process (FC) under $H = 5$ Oe. The magnetization data exhibit a remarkable drop in ZFC at 4.4 K, suggesting the emergence of superconductivity with the transition temperature T_C of 4.4 K. Detailed magnetization and specific heat measurements are able to determine the bulk nature of the superconductivity (the results will be published elsewhere).

To reveal the intrinsic origin of rich magnetism, pure A_2Mo_3N samples are examined by the first-principle calculation. The lattice constants and the internal coordinates of the atoms are optimized [18], and the electronic properties of A_2Mo_3N in the quenched paramagnetic state are studied. Figures 3(c)–3(e) show the total DOS of A_2Mo_3N, and its projection onto A 3(4)d, Mo4d, and N2p orbitals, respectively. It shows that the mixing between A 3(4)d and Mo4d occurs mainly around the Fermi energy ranging from -4 to 2 eV indicating the sizable 3(4) d–4d hybridization between A and Mo orbitals. Particularly, comparable contributions to the

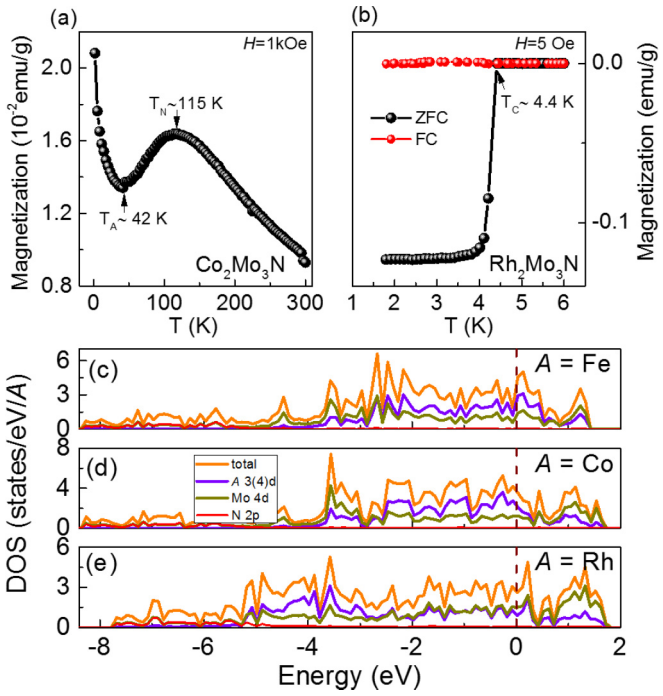

FIG. 3. Variation of magnetization with temperature for (a) Co_2Mo_3N, and (b) Rh_2Mo_3N. T_N marks an antiferromagnetic transition temperature. But, below $T_A = 42$ K, the magnetization increases with the increased temperature, which might be relevant to the paramagnetic phase of small grains. Rh_2Mo_3N shows superconductivity with a transition temperature T_C of 4.4 K. Total DOS and projected DOS on A 3(4)d,Mo4d, and N2p orbitals of the nonmagnetic state of A_2Mo_3N with (c), A = Fe; (d), A = Co; (e), A = Rh.

conducting carriers are witnessed from the Rh4d and Mo4d orbitals in Rh_2Mo_3N, shown in Fig. 3(e). This is attributed to much more extended 4d orbitals of Rh compared to the 3d orbitals of Fe and Co, which leads to a stronger hybridization, expanded bandwidth, and high overlapping between Rh4d and Mo4d orbital states. Quantitatively the values of DOS at the Fermi level are $[N_{\mathrm{Fe}}^{\mathrm{Fe_2Mo_3N}}(Ef) = 2.4$ and $N_{\mathrm{Mo}}^{\mathrm{Fe_2Mo_3N}}(Ef) = 0.73]$, $[N_{\mathrm{Co}}^{\mathrm{Co_2Mo_3N}}(Ef) = 2.3$ and $N_{\mathrm{Mo}}^{\mathrm{Co_2Mo_3N}}(Ef) = 0.8]$, and $[N_{\mathrm{Rh}}^{\mathrm{Rh_2Mo_3N}}(Ef) = 0.67$ and $N_{\mathrm{Mo}}^{\mathrm{Rh_2Mo_3N}}(Ef) = 1.5]$ for Fe_2Mo_3N, Co_2Mo_3N, and Rh_2Mo_3N, respectively, in the unit of states per eV per A(Mo) atom. According to the Stoner criterion [30], magnetism may occur only when the DOS satisfies $N(E_f)I > 1$, where I is the Stoner parameter, which takes values of 0.7–0.9 eV for ions near the middle of the transition metal series. It shows clearly that Mo atoms do not favor magnetism, while Fe and Co atoms contribute significantly and are responsible for magnetisms.

To quantitatively evaluate the strength of the magnetic interactions, we consider the model of nearest-neighbor Heisenberg and DM interactions on the A atom as $H = \sum_{\langle i,j\rangle} J S_i \cdot S_j + \sum_{\langle i,j\rangle} D \cdot (S_i \times S_j)$ where S_i is the operator of A spin at site i; $\langle i,j\rangle$ denotes the summation over the nearest-neighboring sites between A atoms. The parameters J and D are the nearest-neighbor Heisenberg and DM interactions, respectively, and evaluated by using the four-state energy-mapping analysis method [31,32]. The finally calculated parameters J and D are shown in Table S3 [18]. It shows strong ferromagnetism in Fe_2Mo_3N. In contrast, the inclusion of one additional electron in Co not only significantly reduces the strength of the Heisenberg coupling, but also reverses its sign, making the material antiferromagnetic, being consistent with the experimental observations. On the other hand, Rh in Rh_2Mo_3N has very low DOS, and fails to satisfy the Stoner criterion. Although the Mo atom therein has marginal DOS, Rh_2Mo_3N is predicted to be nonmagnetic by our calculation, which is also proved by the experimental observation.

In order to realize skyrmion states, large DM interaction is required, and raising the spin-orbital coupling is one way out [12]. To this end, doping of heavy Rh atoms into the strong ferromagnet Fe_2Mo_3N is a solution. In addition, the more extended Rh4d orbitals make more sufficient overlap to the Mo4d orbital, and further enhance hybridization and the DM interaction. To quantify this understanding, we have substituted one Fe atom in the lattice by Rh, resulting in the phenomenal increase of DM interaction from 2.61 meV in pure Fe_2Mo_3N to 85.77 meV. Unfortunately, such substitution simultaneously introduces large atomic orbital potential difference between large-radii Rh and small-radii Fe atoms, which generates large scattering on itinerant electrons and weakens the exchange interactions. The Heisenberg exchange drops from 379 to 249 meV in the substituted sample. To overcome those potential barriers, an isovalent dopant Co is required. After substituting one Fe atom by Co, the Heisenberg exchange rises to 284 meV. Thus a strong DM coupling with descent Curie temperature is expected in alloy compounds $Fe_xCo_yRh_{2-x-y}Mo_3N$, which is actually what we observed in the magnetization data and Lorentz TEM images.

In conclusion, we have classified helimagnetic materials by symmetry analysis. A new family A_2Mo_3N (A = Fe, Co, and Rh) and their alloy $Fe_xCo_{1.5-x}Rh_{0.5}Mo_3N$ have been suggested to host skyrmions, and are confirmed by the Lorentz TEM measurements. The advantage of this family is the stability under doping. One can dope Pt, Pa, Ni, or other elements to easily tune the magnetic properties such as the enhancement of the Curie temperature [20]. We also expect that the partial substitution of Fe by Ru in Fe_2Mo_3N is also a promising combination for future study. That is because the Ru is isovalent to Fe, but its more extended orbitals and heavy mass would sufficiently enhance the DM interaction. More interestingly, we found the parent phases show ferromagnetic and antiferromagnetic phases for the A = Fe, Co, respectively, and even a possible superconductivity phase in Rh_2Mo_3N. A complete exploration of the phase diagram and stoichiometry is required. More interestingly, due to the lack of inversion symmetry and the elevation of spin-orbital coupling, Rh_2Mo_3N is very like a p-wave superconductor. It is an urgent job to determine its pairing and further investigate the interplay between the skyrmion and superconducting phases. We also hope that this family is just the tip of a huge iceberg. Upon completing this work, we noticed two new skyrmion materials have been proposed [33,34]. They are also included in our framework Table S1 [18]. GaV4S8 is in class N-II, while Co-Zn-Mn is in the same class B-V as our discovery. Other magnetic materials reported in previous works are also worth studying, such as $Fe_{11}C_2$ in space group F_{23} [35], and manganese or iron spinels in group $P4_332$ [36,37].

We thank C. L. Chien, Y. Li, X. M. Xie, and Z. Liu for helpful discussions. This work was supported by the Strategic Priority Research Program (B) of the Chinese Academy of Sciences (Grant No. XDB04040300), the National Natural Science Foundation of China (Grants No. 11227902, No. 11404359, No. 11574322, No. 11374302, No. 11474290, No. 11104281, and No. U1432251), the Foundation for Users with Potential of Hefei Science Center (CAS) through Grant No. 2015HSC-UP001, and Shanghai Yang-Fan Program (Grant No. 14YF1407100).

[1] N. Nagaosa and Y. Tokura, Nat. Nanotechnol. **8**, 899 (2013).
[2] S. Mühlbauer, B. Binz, F. Jonietz, C. Pfleiderer, A. Rosch, A. Neubauer, R. Georgii, and P. Böni, Science **323**, 915 (2009).
[3] X. Z. Yu, Y. Onose, N. Kanazawa, J. H. Park, J. H. Han, Y. Matsui, N. Nagaosa, and Y. Tokura, Nature **465**, 901 (2010).
[4] U. K. Rößler, A. A. Leonov, and A. N. Bogdanov, J. Phys.: Conf. Ser. **303**, 012105 (2011).
[5] X. Z. Yu, N. Kanazawa, Y. Onose, K. Kimoto, W. Z. Zhang, S. Ishiwata, Y. Matsui, and Y. Tokura, Nat. Mater. **10**, 106 (2011).
[6] S. Seki, X. Z. Yu, S. Ishiwata, and Y. Tokura, Science **336**, 198 (2012).
[7] T. Okubo, S. Chung, and H. Kawamura, Phys. Rev. Lett. **108**, 017206 (2012).
[8] S. Heinze, K. von Bergmann, M. Menzel, J. Brede, A. Kubetzka, R. Wiesendanger, G. Bihlmayer, and S. Blügel, Nat. Phys. **7**, 713 (2011).
[9] K. Shibata, X. Z. Yu, T. Hara, D. Morikawa, N. Kanazawa, K. Kimoto, S. Ishiwata, Y. Matsui, and Y. Tokura, Nat. Nanotechnol. **8**, 723 (2013).
[10] H. Du, R. Che, L. Kong, X. Zhao, C. Jin, C. Wang, J. Yang, W. Ning, R. Li, C. Jin, X. Chen, J. Zang, Y. Zhang, and M. Tian, Nat. Commun. **6**, 8504 (2015).
[11] I. Dzyaloshinskii, J. Phys. Chem. Solids **4**, 241 (1958).
[12] T. Moriya, Phys. Rev. **120**, 91 (1960).
[13] A. N. Bogdanov and D. A. Yablonskii, Zh. Eksp. Teor. Fiz. **95**, 178 (1989).
[14] A. Bogdanov and A. Hubert, J. Magn. Magn. Mater. **138**, 255 (1994).
[15] A. N. Bogdanov and D. A. Yablonskii, Sov. Phys. JETP **68**, 101 (1989).
[16] R. R. Birss, *Symmetry and Magnetism*, Selected Topics in Solid State Physics Vol. III (North-Holland Publishing Company, Amsterdam, 1964).
[17] A. Bogdanov and A. Hubert, Phys. Status Solidi B **186**, 527 (1994).
[18] See Supplemental Material at http://link.aps.org/supplemental/10.1103/PhysRevB.93.060409 for details in classifying crystal symmetries, first principle calculations, and magnetometry measurements of alloys with different doping levels.
[19] T. J. Prior and P. D. Battle, J. Solid State Chem. **172**, 138 (2003).
[20] T. J. Prior, S. E. Oldham, V. J. Couper, and P. D. Battle, Chem. Mater. **17**, 1867 (2005).
[21] P. D. Battle, F. Grandjean, G. J. Longc, and S. E. Oldham, J. Mater. Chem. **17**, 4785 (2007).
[22] A. F. Wells, *Three-Dimensional Nets and Polyhedra* (Wiley, New York, 1977).
[23] M. Janoschek, M. Garst, A. Bauer, P. Krautscheid, R. Georgii, P. Böni, and C. Pfleiderer, Phys. Rev. B **87**, 134407 (2013).
[24] H. Wilhelm, M. Baenitz, M. Schmidt, U. K. Rößler, A. A. Leonov, and A. N. Bogdanov, Phys. Rev. Lett. **107**, 127203 (2011).
[25] Y. Onose, N. Takeshita, C. Terakura, H. Takagi, and Y. Tokura, Phys. Rev. B **72**, 224431 (2005).
[26] S. V. Grigoriev, E. V. Moskvin, V. A. Dyadkin, D. Lamago, T. Wolf, H. Eckerlebe, and S. V. Maleyev, Phys. Rev. B **83**, 224411 (2011).
[27] A. Bauer and C. Pfleiderer, Phys. Rev. B **85**, 214418 (2012).
[28] E. Karhu, S. Kahwaji, T. L. Monchesky, C. Parsons, M. D. Robertson, and C. Maunders, Phys. Rev. B **82**, 184417 (2010).
[29] R. Mathieu, Ph.D. thesis, Uppsala University, 2002.
[30] D. J. Singh, Phys. Rev. B **78**, 094511 (2008).
[31] H. J. Xiang, E. J. Kan, S.-H. Wei, M.-H. Whangbo, and X. G. Gong, Phys. Rev. B **84**, 224429 (2011).
[32] M. H. Whangbo, H. J. Koo, and D. Dai, J. Solid State Chem. **176**, 417 (2003).
[33] I. Kézsmárki, S. Bordács, P. Milde, E. Neuber, L. M. Eng, J. S. White, H. M. Rønnow, C. D. Dewhurst, M. Mochizuki, K. Yanai, H. Nakamura, D. Ehlers, V. Tsurkan, and A. Loidl, Nat. Mater. **14**, 1116 (2015).
[34] Y. Tokunaga, X. Z. Yu, J. S. White, H. M. Rønnow, D. Morikawa, Y. Taguchi, and Y. Tokura. Nat. Commun. **6**, 7368 (2015).
[35] C. M. Fang, M. A. Van Huis, and H. W. Zandbergen, Comput. Mater. Sci. **51**, 146 (2012).
[36] W. Brandford, M. A. Green, and D. A. Neumann, Chem. Mater. **14**, 1649 (2002).
[37] L. A. de Picciotto and M. M. Thackeray, Mater. Res. Bull. **21**, 583 (1986).